Assessment of Vascular Network Segmentation

Jack Collins collinja@mail.nih.gov
ABCC-ISPSAIC-Frederick, Inc., NCI-Frederick
Frederick, 21702, USA

Christopher Kurcz kurczce@mail.nih.gov
ABCC-ISPSAIC-Frederick, Inc., NCI-Frederick
Frederick, 21702, USA

Curtis Lisle curtislisle@knowledgevis.com
KnowledgeVis LLC
Maitland, 32751, USA

Yanling Liu liuy5@mail.nih.gov
ABCC-ISPSAIC-Frederick, Inc., NCI-Frederick
Frederick, 21702, USA

Enrique Zudaire zudairee@mail.nih.gov
Angiogenesis Core Facility, NCI
NIHGaithersburg, 20877, USA

Abstract

We present an analysis framework to assess the quality and accuracy of vessel segmentation algorithms for three dimensional images. We generate synthetic (in silico) vessel models which act as ground truth and are constructed to embody varying morphological features. These models are transformed into images constructed under different levels of contrast, noise, and intensity. To demonstrate the use of our framework, we implemented two segmentation algorithms and compare the results to the ground truth model using several measures to quantify the accuracy and quality of segmentation. Furthermore, we collect metrics which describe the characteristics of the vessels it fails to segment. Our approach is illustrated with several examples. Funded by NCI Contract No.HHSN261200800001E.

Keywords: Vessel Segmentation, Network Comparison, Quantitative Analysis, Segmentation Quality, Segmentation Accuracy.

1. INTRODUCTION

Extracting vascular networks from three dimensional images remains a difficult and exciting challenge. Many segmentation algorithms have been designed to target different types of vasculature imaged using various modalities and are applied to a wide range of problems in disease diagnosis, flow dynamics, surgical planning, etc... (see e.g. [2][1][3]). Despite the sophistication of these methods, it is often difficult to choose a particular segmentation algorithm given a collection of similar images since a given method may make implicit assumptions about image or vessel characteristics. Furthermore, it is not clear how to predict or quantify the quality or accuracy of a given method onthose images due to a lack of ground truth data.

In this paper, we provide a methodology to quantify the accuracy and effectiveness of a vessel segmentation algorithm. We provide tools for constructing a model vessel tree which defines the vessel centerline locations and vessel radius and serves as ground truth. This model is transformed into an image with specified contrast, noise and intensity profile and serves as input to the segmentation algorithm under scrutiny. At a minimum we require the segmentation algorithm to produce a binary image depicting vessel location. Additional data including vessel radius, curvature, and local coordinate system may also be specified. This data is then transformed into a graph (network) representation and aligned with the model tree to determine the quality and accuracy of segmentation. We illustrate these operations in Figure 1.

We emphasize that our approach quantifies segmentation quality and accuracy by comparing attribute graphs and not images. By using the model vessel tree as a starting point and simulating the imaging process we can assess the performance of a segmentation algorithm under a variety of image characteristics. Furthermore, we do not require a trained observer to extract the centerlines from a gold standard data set since the model vessel tree contains centerline location as an attribute. Morphological features (e.g. vessel radius, curvature, tortuosity, etc...) are maintained as attributes of the model vessel tree and we can assess the segmentation performance as a function of these features.

We provide metrics describing the correctly segmented vessels, missed vessels, false positives and changes in network topology to assess segmentation quality. Beyond the quality assessment, we determine the accuracy of segmentation by computing the deviation of the centerline and radius between the ground truth model and the segmentation estimation. Additional assessment includes collecting features where that algorithm fails (e.g. did the algorithm fail to detect thin or highly curvedvessels?). Thus, we provide a framework to determine how well a particular segmentation algorithm performs as a function of the image quality defined by contrast, noise, and intensity profile. This paper is organized as follows. In Section 2, we describe the model tree creation, transformation of the model tree to an image, segmentation of the image, and comparison of the segmented result to the model. Next, in Section 3, we perform a quality and accuracy assessment for several models. Finally, in Section 4, we summarize the results for the different models and describe possible extensions and improvements to our approach.

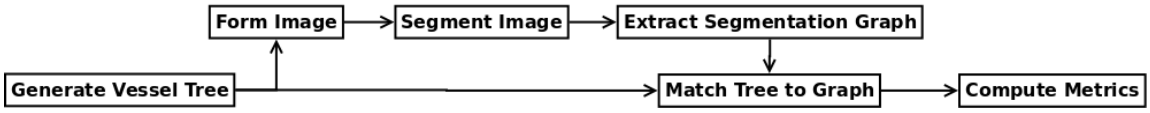

FIGURE 1: Flow Chart of Major Operations in Vessel Segmentation Assessment Framework

2. MATERIALS AND METHODS

In this section we describe the process of model vessel tree generation, model tree to image formation, segmentation of vessels from a noise corrupted image, and a method to compare the model to the segmentation result.

2.1 Model Tree Generation

We construct model vessel trees which serve as ground truth for subsequent analysis. Lindenmayer systems [17][18] (*L*-systems) provide a natural framework for defining such objects. This formalism grows a tree from a root location by following a set of rules which specify the direction of growth, branch radius, branch length, angle between branches and number of branches. In Figure 2 we illustrate this procedure with a simple example. We note that *L*-systems have been used in a variety of applications in computational botany, computer graphics, and medicine (see e.g. [10][24][20][21]). Although our model is formally a tree, there is no fundamental limitation for its extension to a more complicated topology.

A model tree contains a collection of nodes (vertices), connections between nodes (edges), and node attributes. We characterize these trees by node location (x, y, z coordinates), radius, node spacing and node type i.e. end, middle, or junction. Furthermore, we generate a local coordinate system at each node given by the tangent vector $(T(s))$, normal vector $(N(s))$, and binormal vector $(B(s))$ where s is arc length. These vectors are used to compute the curvature$(\langle dT/ds, N \rangle)$andtorsion $(\langle dB/ds, N \rangle)$ at each node location.

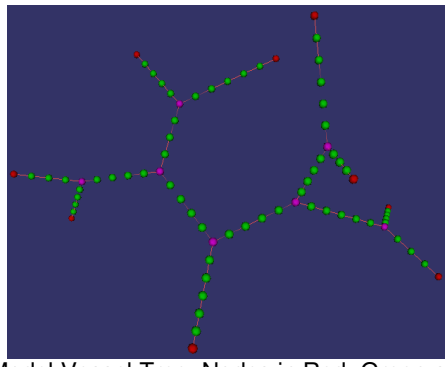

FIGURE 2: Simple Example of Model Vessel Tree. Nodes in Red, Green and Magenta Correspond to End, Middle and Junctions (Respectively).

2.2 Image Generation From Model Tree

We transform a model vessel tree to a volumetric image by simulating the image formation process. This mapping requires specification of spatial resolution, intensity range of the vessel, background intensity, noise level, and intensity profile of the vessel cross-section.

To generate the image, we first convert the vessel model to a binary image by rounding each node location in the model to the nearest voxel index. Then to create vessel thickness, we label all voxels inside the sphere given by each nodes radius. Next, this label map is convolved with a Gaussian (characterized by its standard deviation η) which blurs the boundary of the vessel producing a smooth cross-section intensity profile. At this point we have an image of real values in $[0, 1]$ where the values close to one correspond to the interior of large vessels and values close to zero correspond to either the exterior of vessels or the centerline of thin vessels. We use a linear mapping to a specified vessel intensity maximum and minimum $([0, 1] \rightarrow [I_{min}, I_{max}])$ and add a background intensity (I_{back}) to the image. Finally, we complete the process by corrupting the image with additive Gaussian noise (characterized by its standard deviation σ). The image formation steps are illustrated in Figure 3.

This image formation process characterizes images by four simple qualities (i) the relationship between voxel intensities and vessel radius, (ii) contrast between vessel centerline and background, (iii) amount of noise relative to contrast and (iv) the ratio of node spacing to image resolution. Thus, a wide range of images can be created simulating different image acquisition environments.

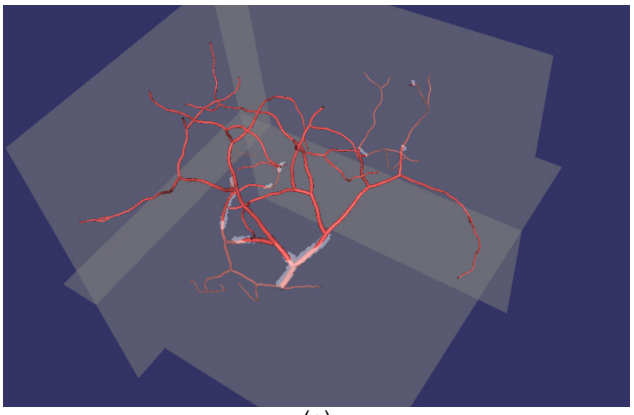

(a)

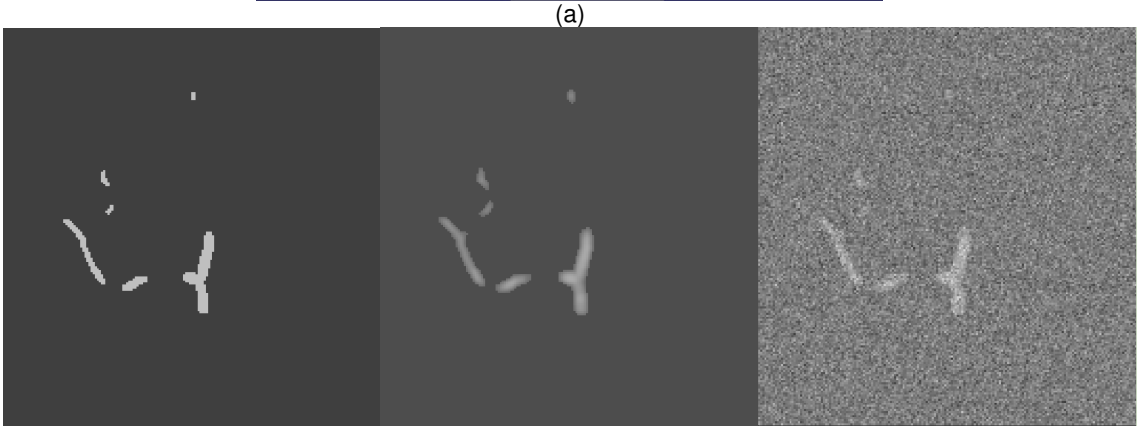

(b) (c) (d)

FIGURE 3: Image Formation Process. (a) Generated x, y, z Slices of Label Map Overlayed on Model Tree. For Visualization Purposes The Model Has Been Made Artificially Thinner. (b) A Slice From The Label Map. (c) Slice From (b) After Gaussian Smoothing $(\gamma = 2)$, Intensity Rescaling $(I_{min} = 200, I_{max} = 400)$ and Background Added $(I_{back} = 100)$. (d) Slice From (c) After Addition of Gaussian Noise $(\sigma = 100)$.

2.3 Vessel Segmentation

There is a vast amount of literature and wide range of methods for vessel segmentation (see e.g.[13][19] for a review). We emphasize that the main point of this paper is not the development of vessel segmentation algorithms but the assessment of their performance. Toward this end, we implemented two vessel segmentation algorithms for demonstration purposes. In what follows, we denote $I(x)$ the image intensity at position $x \in \mathbb{R}^3$.

2.3.1 Vesselness

The first segmentation method assumes a cylindrical model for vessels and uses the eigenvalues of the Hessian matrix to enhance vessel voxels (see e.g. [7][25]). We begin by considering the voxels above a specified threshold $(\{x | I(x) > \epsilon_1\})$. For each specified scale, τ, we form the Hessian matrix

$$H_\tau(x) = \tau^2 \begin{pmatrix} \partial_{xx} G_\tau * I & \partial_{xy} G_\tau * I & \partial_{xz} G_\tau * I \\ \partial_{yx} G_\tau * I & \partial_{yy} G_\tau * I & \partial_{yz} G_\tau * I \\ \partial_{zx} G_\tau * I & \partial_{zy} G_\tau * I & \partial_{zz} G_\tau * I \end{pmatrix} \tag{2.1}$$

where $G_\tau(x) = 1/(2\pi\tau^2)^{3/2} e^{-\|x\|^2/2\tau^2}$, $*$ denotes the convolution operator, and ∂_x denotes the partial derivative with respect to x. The eigenvalues of (2.1) are computed and ordered so that $|\lambda_{1,\tau}| \leq |\lambda_{2,\tau}| \leq |\lambda_{3,\tau}|$. For each scale, we compute

$$V_\tau(x) = \begin{cases} 0, \ \lambda_{2,\tau} > 0 \ or \ \lambda_{3,\tau} > 0 \\ \left(1 - e^{-\frac{R_A^2}{2\alpha^2}}\right) e^{\frac{R_B^2}{2\beta^2}} \left(1 - e^{-\frac{S^2}{2\gamma^2}}\right), \ otherwise \end{cases} \tag{2.2}$$

where $c_\tau = \sqrt{\lambda_{1,\tau}^2 + \lambda_{2,\tau}^2 + \lambda_{3,\tau}^2}$, $b_\tau = |\lambda_{1,\tau}|/\sqrt{\lambda_{2,\tau}\lambda_{3,\tau}}$ and $a_\tau = |\lambda_{2,\tau}|/|\lambda_{3,\tau}|$. Finally, we determine the vesselness, $V(x) = max_\tau V_\tau(x)$, and construct a label map, $L_V = \{x | V(x) \geq \epsilon_V\}$, by considering the voxels above a specified vesselness threshold, ϵ_V.

2.3.2 Fast Marching

The second segmentation method uses the Fast Marching method (see e.g. [27][12, §9.3.1]). This method propagates an outward moving front satisfying

$$|\nabla T| F(x) = 1 \tag{2.3}$$

from an initial surface S given a speed $F(x)$. The solution, T, to (2.3) represents the arrival time at location x. We use a sigmoidal speed function,

$$F(x) = \frac{1}{1 + e^{-\frac{A(x) - K}{\beta}}}$$

where $A(x)$ is the average intensity over a $3 \times 3 \times 3$ neighborhood. To construct the label map, $L_F = \{x | T(x) \leq \epsilon_F\}$, we consider all voxels whose arrival time is less than a specified threshold, ϵ_F.

2.3.3 Post Processing

To aid subsequent analysis we apply the hole filling algorithm [12, §6.6.4] to the label map constructed from either segmentation algorithm (L_V or L_F). We determine the vessel centerline using the skeletonization algorithm [9] and the vessel radius at each centerline location using the distance transform [31].

From the labeled centerline image we generate a data structure which contains the locations of the vessel centerline at each point and refer to this structure as the *segmentation graph* throughout the rest of this paper. We note that its topology may deviate from a tree due to segmentation errors. The segmentation graph is constructed by converting each centerline voxel to a node in the segmentation graph where the node location is given by the voxels physical coordinates. The remaining attributes of the graph are then populated. Since the model has been discretized during the image formation process, the node locations in the segmentation graph may not align with those from the model. In Figure 4 we provide an example, where the spacing between points in the model is 1 but, the spacing between points in the segmentation graph is either 1, $\sqrt{2}$ or $\sqrt{3}$.

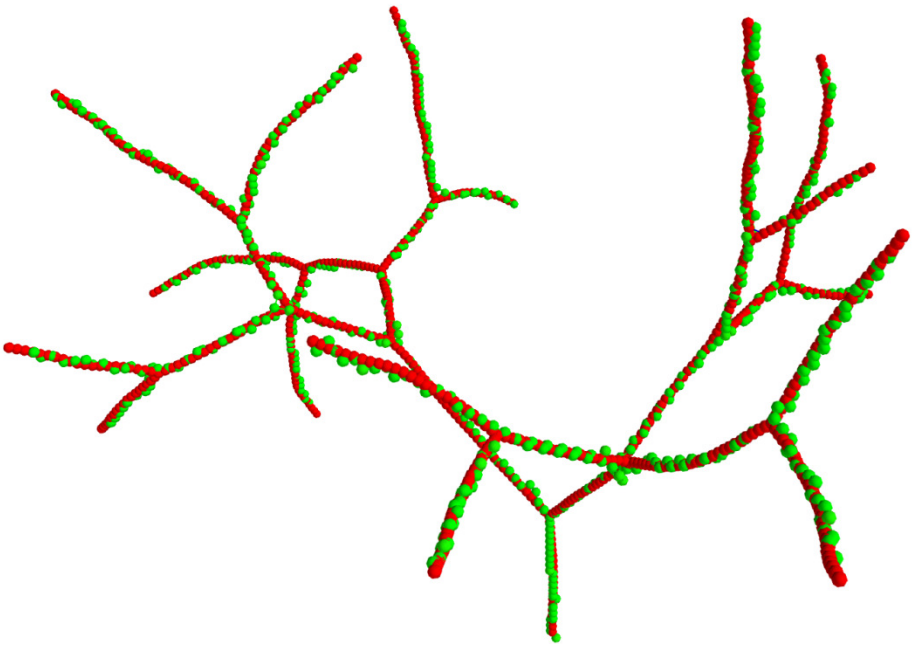

FIGURE4: Model Tree in Red and Segmentation Graph in Green

2.4 Graph Matching

Given a model tree and a segmentation graph we determine the nodes in the segmentation graph that correspond to these in the model tree. This mapping allows us to compare results of segmentation to ground truth. Since the spacing between nodes in the model tree and vessel graph may differ, we use a many-to-one mapping between nodes in the segmentation graph to nodes in the model tree.

This association problem is often referred to as inexact graph matching (see e.g. [4][6][30][32]) which is often posed as a global alignment problem or largest subgraph isomorphism problem. However, the problem presented here is slightly different because we have node attribute information which can be used to assist in the association problem. Thus, we seek a method which optimizes the global alignment while minimizing the pairwise distance between nodes in the model tree and segmentation graph.

For this purpose, we use the IsoRank algorithm [28] which constructs a set of constraints for all pairs of nodes in the model tree and segmentation graph based on neighborhood information. Using these constraints and minimizing the pairwise distances, the IsoRank algorithm establishes a ranking between pairs of nodes in the model tree and segmentation graph. We note that the rankings are computed by solving for the largest eigenvalue of a sparse matrix and the entries of the eigenvector correspond to the pairwise ranks (as in the PageRank algorithm see e.g. [16]). The ranking matrix in combination with a maximum allowable deviation between node positions and maximum number of multiple matches is uses to determine the many-to-one mapping between nodes in the segmentation graph to nodes in the model tree. An example matching is illustrated in Figure 5.

Given the association between nodes in the model tree and segmentation graph we classify nodes in the segmentation graph as either matched, missed or false positives. A matched node in the segmentation graph is associated with one node in the model tree, a missed node in the model tree has no association with a node in the segmentation graph and a false positive is a node in the segmentation graph with no association to a node in the model tree. Notice in Figure 5 thatin a limited number of cases the algorithm can fail to match nodes that appear to correspond to a node in the model tree. We note that this occurs due to our enforcement of a many-to-one mapping. Adopting a many-to-many matching policy would reduce the number of false positives at the cost of matching nodes that may not correspond. Finally, a one-to-one policy would inflate the number of missed nodes since the spacing between nodes in the model tree is less than or equal to the spacing in the segmentation graph.

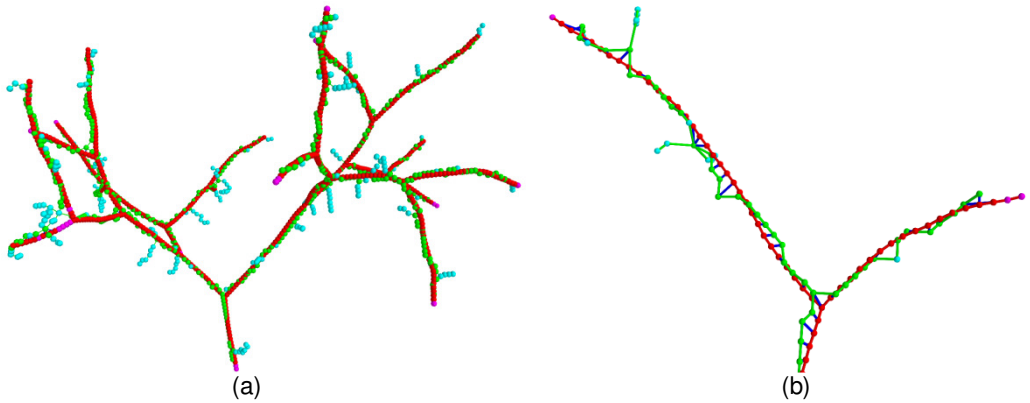

(a) (b)

FIGURE5: Model Tree and Segmentation Graph Matching. (a) Model Tree Nodes in Red, Segmentation Graph Nodes in Green, Association Between Matched Nodes as Dark Blue Cylinders, Missed Nodes in Magenta, False Positives in Light Blue. (b) Close up of (a).

3. RESULTS

In this section we construct two distinct model trees, generate images under a variety of conditions, and compare the segmentation graph to the model tree for the purpose of quantifying segmentation quality and accuracy for the vesselness and fast marching algorithms. The segmentation quality metrics include the (i) the percentage of correctly matched nodes, (ii) identification of the missed node type (i.e. junction, middle or end), (iii) percentage of false positives and (iv) the amount of topological change between model tree and segmentation graph. For the matched nodes, we compute the position and radius accuracy and, furthermore, record the curvature and radius of missed nodes in the segmentation graph. Therefore, this analysis measures how well each segmentation algorithm performs and quantifies the characteristics of vessels each algorithm fails to segment.

We present the quality measures as bar charts displaying the percentage of matched and missed model nodes (see Figures 7(a,d), 11(a,d)). In a similar fashion, we display the percentage of false positives i.e. the number of unmatched segmentation nodes over the total number of model nodes (see Figures 7(b,e), 11(b,e)). We note that the matching algorithm systematically over estimates the number of false positives due to the many-to-one constraint described in Section 2.4. Unfortunately, we do not have a rigorous bound for the error induced but can get a rough estimate by examining the number of false positives under no noise. To measure the quality with respect to changes in the topology we use a bar chart to display the percentage of nodes in each connected component of the segmentation graph (see Figures 7(c,f), 11(c,f)). Recall that a connected component of a graph is a subgraph which contains a path between every pair of nodes. For example, in Figure 7(c) with $\sigma = 0$ there are 4 connected components with the largest component containing approximately 95 percent of the segmentation graphs nodes.

The position accuracy of matched nodes is computed using the max-norm $(\|x\|_\infty = max_i|x_i|)$. Since a vector with unit max-norm is bounded by a box of side length one, it facilitates a straightforward comparison to voxel coordinates. The position accuracy includes error from the quantization of the nodes position during the image formation process and error due to segmentation inaccuracy. To compute the position accuracy, we calculate the distance between every pair of matched nodes and note that due to the many-to-one mapping of segmentation nodes to model nodes we systematically over estimate the position error. In practice, however, we expect the number of many-to-one mappings to be small (compared to the total number of nodes in the model) and thus the effect is minimal. We display the position accuracy as a histogram where the *x*-axis denotes the error between model and segmentation node position and on the *y*-axis we display the number of nodes for each bin. We overlay the results from several levels of noise using different colors (see Figures 8(a,c), 12(a,c)). A similar plot is provided for the relative radial error (see Figures 8(b,d), 12(b,d)).

We also characterize the missed nodes by radius and curvature with a histogram plot. In this plotthe *x*-axis corresponds to the value of radius (curvature) and *y*-axis corresponds to the percentageof nodes within a radius (curvature) bin that were missed by the segmentation algorithm. We overlaythe results from several levels of noise using different colors (see Figures 9(a,c)(b,d), 13(a,c)(b,d)).

The model trees shown in Figures 6 and 10 share similar topological features but have differentmorphologies. In particular, the models in Figure 6 and Figure 10 differ significantly only inthe curvature of the branches. In fact, the image generation process and segmentation algorithmused identical parameters.

In what follows, we generate images of the model trees (see Section 2.2) with vessel intensity range of $[I_{min} = 200, I_{max} = 400]$, background intensity of $I_{back} = 100$, smoothing factor $\eta = 2$,noise levels $\sigma = 0, 20, 40, 60, 80, 100, 120,$ and spacing between nodes and image resolution of 1.We use the same segmentation parameters for each model. For the vesselness algorithm (seeSection 2.3.1), we use an intensity threshold $\epsilon_I = 150$, six logarithmically spaced

scales (τ) from 1 to5, vesselness parameters $\alpha = 0.25, \beta = 0.25$ and $\gamma = 30$, and a vesselness threshold $\epsilon_V = 0.75$.As a post processing step we removed all components with five nodes or less that contain no junctionpoints. For the fast marching algorithm (see Section 2.3.2) we use speed function parameters $\mu = 1$and $\kappa = 180$, a time threshold $\epsilon_F = 500$, and one seed point at the root location of the tree as theinitial contour. To generate the hole filled label map (see Section 2.3.3) we use a majority threshold0 and a maximum of 20 iterations. For the IsoRank algorithm we set $\alpha = 0.5$ (see [28, equation 5]),a maximum of 3 matches of a segmentation node to a model node and a maximum distance of 3 fora match.

3.1 Model Tree 1

This model has 726 nodes with radii between 0.6 and 4. Both algorithms correctly segment an overwhelming majority of nodes with the fast marching algorithm having a slightly greater percentage of matched nodes. The vesselness algorithm induces a larger percentage of false positives and fragments the model tree into several components with the number of components increasing as the noise level increases (see Figure 7). The number of matched nodes generated by the vesselness algorithm tends to decrease as the noise level increases whereas the number of matched nodes generated by the fast marching algorithm is nearly invariant to noise level.The position and radius accuracy are not significantly affected by the amount of noise and the algorithmsperform equally well with regard to the position accuracy. The vesselness algorithm performsslightly better with regards to radius accuracy (see Figure 8). Almost all matched nodes are accurateto within one voxel and approximately 50 percent are inside a box of side length $1/2$ (seeFigure 8(a,c)). The fast marching algorithm generally over estimates the vessel radius since weuse the average intensity over a $3 \times 3 \times 3$ window when evaluating the speed function, and, thusartificially extend the boundary of the vessel.

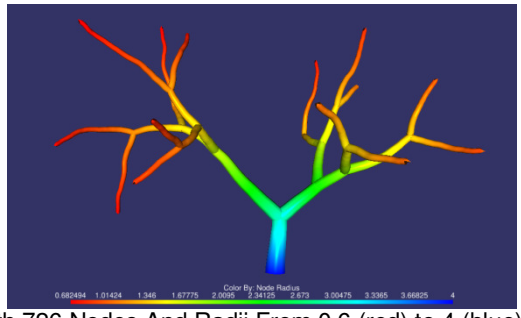

FIGURE 6: Model Tree 1 With 726 Nodes And Radii From 0.6 (red) to 4 (blue). Image of Model Tree Has A Maximum Intensity of 400, A Minimum Intensity of 200 And A Background Intensity of 100.

The fast marching algorithm generates fewer false positives then the vesselness algorithm. Furthermore,the vesselness algorithm tends to produce several components while the fast marchingalgorithm produces only one. The behavior is expected as the fast marching algorithm cannot splitthe contour into multiple closed contours and the vesselness algorithm does not enforce connectivityconstraints. Thus, false positives generated by the fast marching algorithm correspond to additionalshort branches and for the vesselness algorithm correspond to additional components.

The majority of missed nodes have small radii and their percentage increases with the level of noise(see Figure 9(a,c)). In some conditions, we observe that the missed nodes correspond to thosenear the root (see Figure 9(c)). An expected result is that nodes with larger curvature are morelikely to be missed and the percentage increases with the level of noise (see Figure 9(b,d)). Bothalgorithms tend to miss nodes with similar properties and in similar percentages.

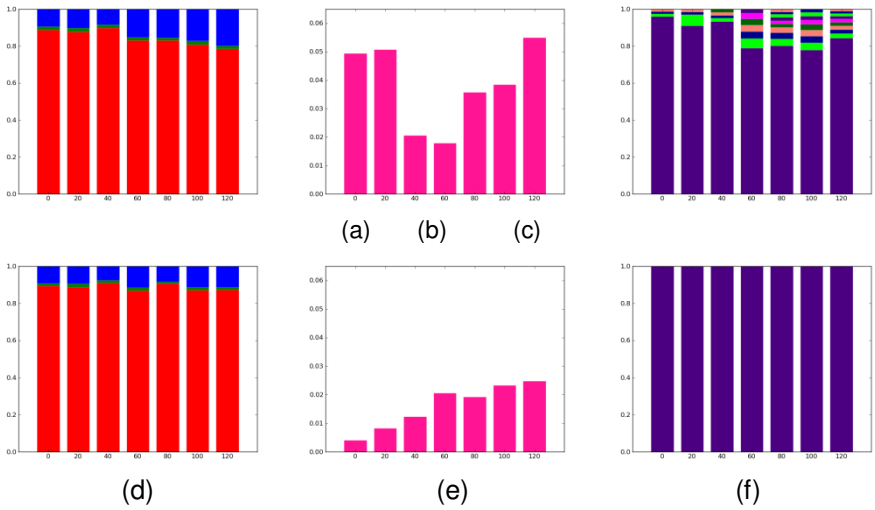

FIGURE 7: Quality Results Associated With The Model in Figure 6. Top Row Corresponds to Results From The Vesselness Algorithm And The Bottom Row From Fast Marching Algorithm. (a,d) Percentage of Correctly Segmented Nodes (red), Missed Junction Nodes (cyan), Missed End Nodes (green), And Missed Middle Nodes (blue) As A Function of Noise Level ($\sigma = 0, 20, 40, 60, 80, 100, 120$). (b,e) Percentage of False Positives As A Function of Noise. (c,f) Percentage of Nodes Within Each Component of The Segmentation Graph. Each Color Corresponds to A Component.

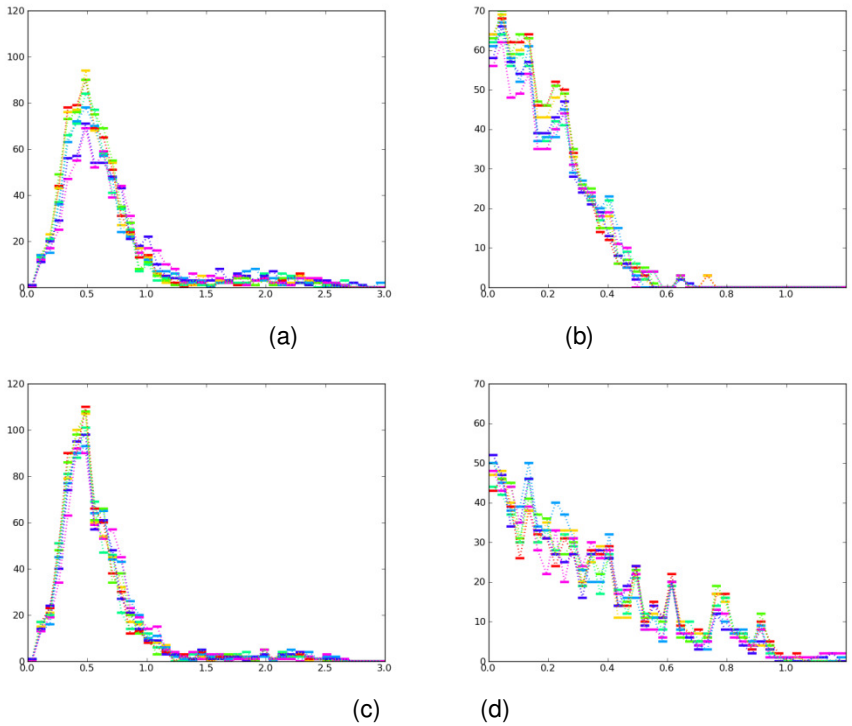

FIGURE 8: Accuracy Results Associated With The Model in Figure 6. Top Row Corresponds to Results From The Vesselness Algorithm And The Bottom Row From Fast Marching Algorithm. Each Histogram Corresponds to The Noise Level 0-red, 20-yellow, 40-green, 80-light blue, 100-dark blue, 120-magenta. (a,c) Absolute Position Error (Using max-norm) Between Every Pair of Matched Nodes. (b,d) Relative Radius Error Between Every Pair of Matched Nodes.

3.2 Model Tree 2

This model has 769 nodes with radii between 0.8 and 3 and is similar to themodel described in Section 3.1 except the vessels are more curved. We compare the quality andaccuracy results to those in Section 3.1 for the purpose of assessing the sensitive of each vesselsegmentation algorithm to curvature.

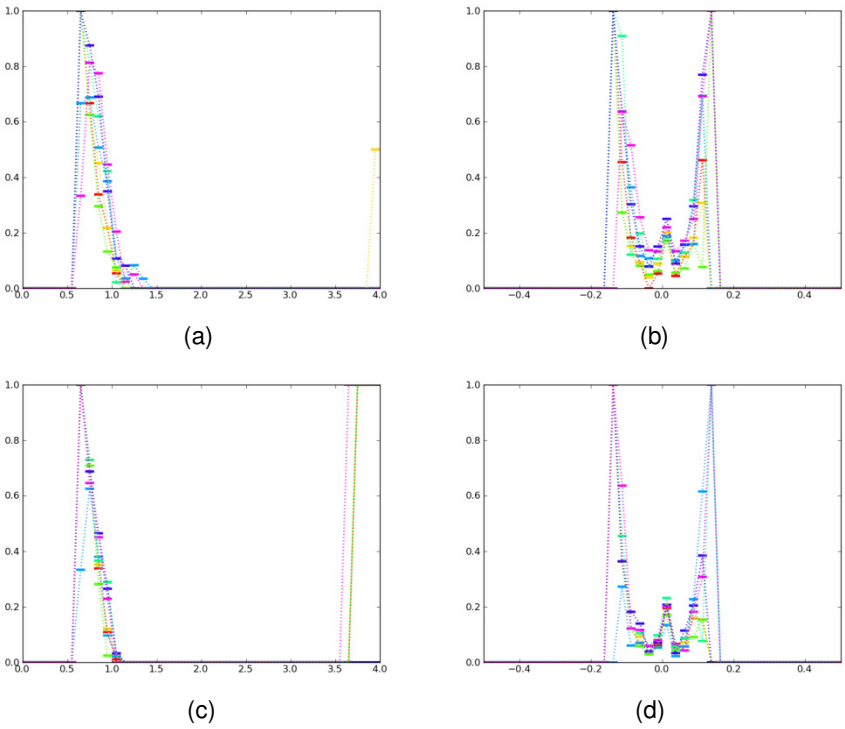

FIGURE 9: Properties of Missed Nodes Associated With The Model in Figure 6. Top Row Corresponds to Results From The Vesselness Algorithm And The Bottom Row From Fast Marching Algorithm. Each Histogram Corresponds to The Noise Level 0-red, 20-yellow, 40-green, 80-light blue, 100-dark blue, 120-magenta. (a,c) Percentage of Missed Nodes Within Radius Interval. (b,d) Percentage of Missed Nodes Within Curvature Interval.

Each algorithms number of matched nodes, false positives and components is essentially the sameas in Section 3.1 (see Figure 11(a,b,c)). The vesselness algorithm produces two large componentswhen $\sigma = 60, 100$ (see Figure 11(c)). In this case, these components are created because of high levels of noise located at a middle branch yielding low vesselness responses. Furthermore, since the eigenvalues of (2.1) are sensitive to changes incurvature (see [15]) we expect the segmentation graph to miss more nodes in curved region andthus create more components in the graph.

The position and radius accuracy follow similar trends as those in Section 3.1 (see Figure 12). Highlycurved nodes are missed as the noise level increases (see Figures 13(b,d)), however, it is difficult tomake a direct comparison because a percentage of missed nodes is given (not an absolute number)and range of curvatures in the two models varies significantly.

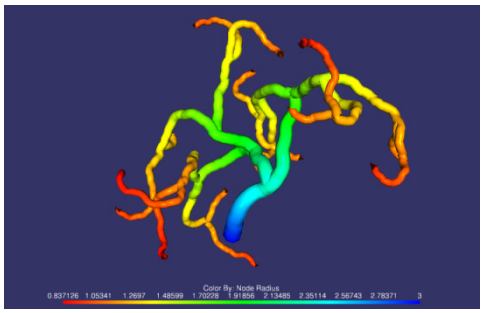

FIGURE 10: Model Tree 2 With 769 Nodes And Radii From 0.8 (red) to 3 (blue). Image of Model Tree Has A Maximum Intensity of 400, A Minimum Intensity of 200 And A Background Intensity of 100.

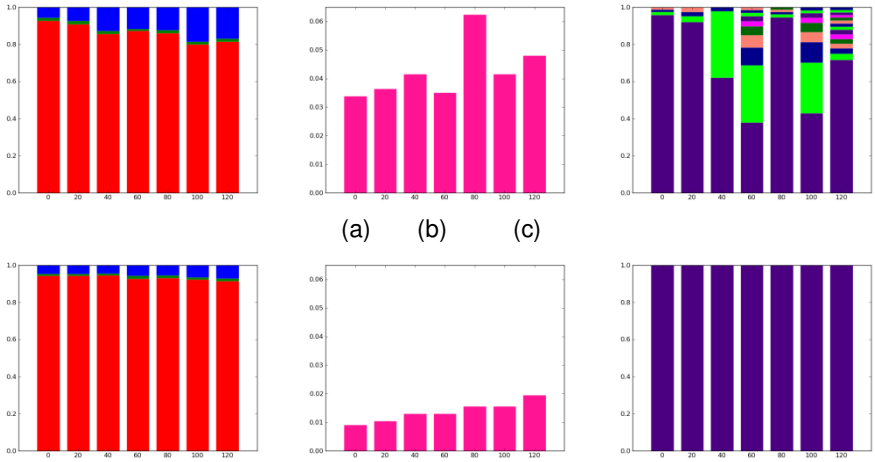

(a) (b) (c)

(d) (e) (f)

FIGURE 11: Quality Results Associated With The Model in Figure 10. Top Row Corresponds to Results From The Vesselness Algorithm And The Bottom Row From Fast Marching Algorithm. (a,d) Percentage of Correctly Segmented Nodes (red), Missed Junction Nodes (cyan), Missed End Nodes (green), And Missed Middle Nodes (blue) As A Function of Noise Level ($\sigma = 0,20,40,60,80,100,120$). (b,e) Percentage of False Positives As A Function of Noise. (c,f) Percentage of Nodes Within Each Component of The Segmentation Graph. Each Color Corresponds to A Component.

4. DISCUSSION

We have developed model vessel trees and a quantitative analysis framework to assess the accuracyand quality of vessel segmentation algorithms for three dimensional images. We applied thisframework to two models under varying image qualities using two segmentation algorithms of fundamentallydifferent classes. The results of this assessment can be briefly summarized by (i) bothalgorithms have roughly the same quality with respect to the number of correctly segmented nodes(ii) the vesselness algorithm introduces a significantly larger number of false positives (iii) the vesselnessalgorithm fragments the model tree into several components while the fast marching algorithmretains the tree structure and (iv) the segmentation quality degrades as the vessels become more thin and/or curved. This type of quantitative result is not surprising as the vesselness algorithm implicitlyassumes a cylindrical model and the fast marching algorithm can only move the contour inan outward normal direction and cannot break the closed contour. More importantly, this analysisprovides qualitative information on how and where the algorithm fails.

We would like to point out similar work in [26] where the authors developed a framework for characterizingand comparing coronary artery centerline extraction algorithms. In this work the authorsassembled a publicly available database of Computed Tomography Angiography (CTA) images andderived the ground truth centerline from three trained observers. The images were acquired using astandard protocol and algorithms where ranked based on overlap and accuracy metrics. The majordifference with our approach is that we start with model generation which

defines ground truth ratherthan extracting the vessel tree from the image. This luxury allows us to easily identify the vesselfeatures that the algorithm fails to segment. Furthermore, we do not need to merge the centerlinetraced by each observer and determine the uncertainty this induces.

Generally, we expect this framework to be used as a measure of performance tool for the assessmentof vessel segmentation algorithms under a wide range of scenarios. Depending on the applicationthe vessel segmentation algorithm may apply different principles. For example, techniques to segmentthe coronary artery may significantly vary from algorithms used to extract capillary beds (see e.g. [1][34][23][29]). With the generation of appropriate models, algorithms designed for either casecan be assessed using our framework. Thus, as one designs a segmentation algorithm it is possibleto quickly assess the impact of differing implementations or parameters. Another use of thisframework is to quantify the limits of detectability for a particular algorithm. As shown in Section 3,analysis of missed node distributions versus vessel radius is straightforward and could be extendedto incorporate other image, topological, or morphological properties (e.g. tortuosity, segment length,degree distribution, etc...). This type of analysis is particularly interesting when the imaging deviceis well characterized. In this case, the image generation process can be modified to better modela particular imaging modality. Thus, a candidate segmentation algorithm can be fully characterizedagainst a particular class of data. Although beyond the scope of this paper, we note that our approach may be used for other network structures e.g. neural networks. In this case the metrics of interest may be more closely related to network topology than morphological properties. Finally, given a vessel network, a segmentation algorithm and adesired quality result, one may determine the required image characteristics. This may assist in thedevelopment of imaging protocols with the intention of subsequent quantitative analysis and not justvisual clarity. For example, one may anticipate the need to accurately segment vessels of a certainradius (for a particular problem a biological argument may be made) and may want to ascertain theimage quality required so that a particular segmentation algorithm performs at a given quality level.

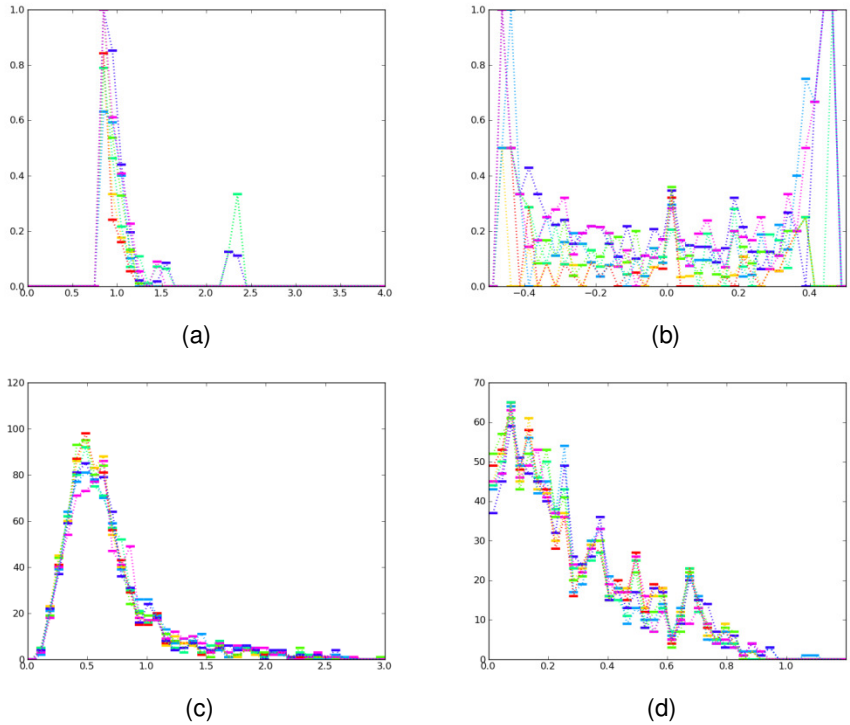

FIGURE 12: Accuracy Results Associated With The Model in Figure 10. Top Row Corresponds to Results From The Vesselness Algorithm And The Bottom Row From Fast Marching Algorithm. Each Histogram Corresponds to The Noise Level 0-red, 20-yellow, 40-green, 80-light blue, 100-dark blue, 120-magenta. (a,c) Absolute Position Error (Using max-norm) Between Every Pair of Matched Nodes. (b,d) Relative Radius Error Between Every Pair of Matched Nodes.

We note that several improvements can be made to our framework and categorize them into modelimprovements and analysis improvements. Depending on the application, a more detailed vascularmodel may be desired than the simple *L*-system approach employed here (see e.g. [14]). For example,a study in segmentation algorithms pertaining to angiogenesis could benefit from a vesselmodel which more accurately reflects the vascular morphology in or near the tumor environment.Such methods typically use a system of reaction diffusion partial differential equations (see e.g. [5])to model the growth of a vessel network. If the imaging modality is well characterized, a better suited noise model (rather than additive Gaussian noise) can be implemented. As pointed out in [33] aGaussian smoothed vessel cross section may be insufficient. Since generating the image from themodel is explicit in our framework, changing the type of convolution or averaging procedure to producea particular type of vessel cross section profile is straightforward. Our model currently neglectsbackground objects and does not explicitly incorporate vessel proximity to one another. A naturalextension to our assessment is multivariate analysis of several properties. For example, we couldexamine if missed nodes have a correlation between radius, curvature or contrast.

The software developed in this paper was written using the following free and open source libraries:Insight Toolkit [12] for image processing tasks, NetworkX [8] for the graph representation, Matplotlib[11] for 2D plotting, and Mayavi [22] for 3D plotting.

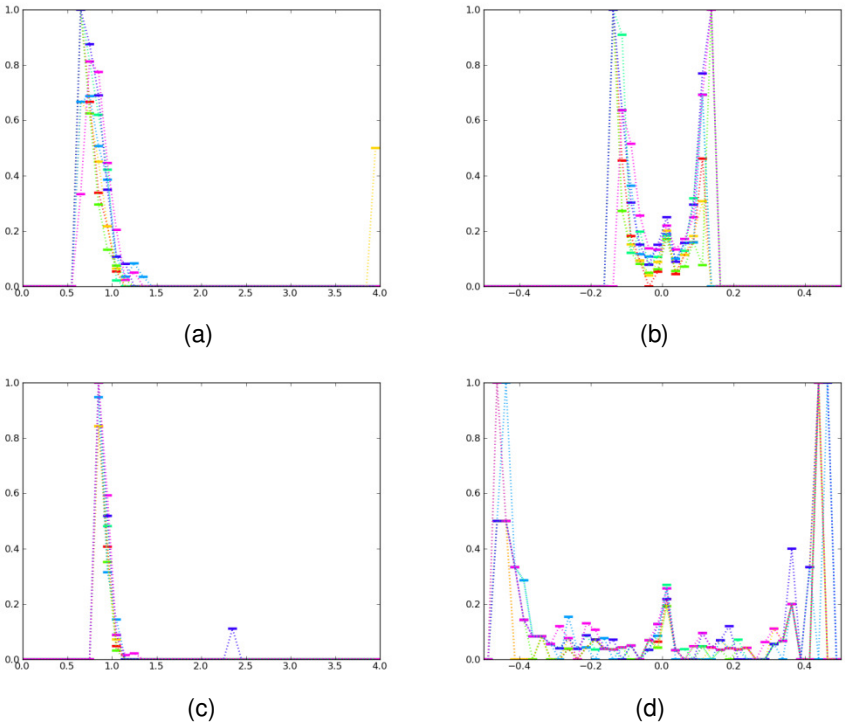

FIGURE 13: Properties of Missed Nodes Associated With The Model in Figure 10. Top Row Corresponds to Results From The Vesselness Algorithm And The Bottom Row From Fast Marching Algorithm. Each Histogram Corresponds to The Noise Level 0-red, 20-yellow, 40-green, 80-light blue, 100-dark blue, 120-magenta. (a,c) Percentage of Missed Nodes Within Radius Interval. (b,d) Percentage of Missed Nodes Within Curvature Interval.

ACKNOWLEDGMENT
This project has been funded in whole or in part with federal funds from the National Cancer Institute, National Institutes of Health, under Contract No. HHSN261200800001E. The content of this publication does not necessarily reflect the views or policies of the Department of Health and

Human Services, nor does mention of trade names, commercial products, or organizations imply endorsement by the U.S. Government.

5. REFERENCES

1. L. Antiga, M. Piccinelli, L. Botti, B. Ene-Iordache, A. Remuzzi, and D. A. Steinman. *"An image-based modeling framework for patient-specific computational hemodynamics"*. Medical & Biological Engineering & Computing, 46:1097-1112, November 2008.

2. E. Bullitt, M. Ewend, J. Vredenburgh, A. Friedman, W. Lin, K. Wilber, D. Zeng, S. R. Aylward, and D. Reardon.*"Computerized assessment of vessel morphological changes during treatment of glioblastoma multiforme: report ofa case imaged serially by MRA over four years"*. Neuroimage, 47(Supplement 2):T143-151, August 2009.

3. F. Cassot, F. Lauwers, C. Fouard, S. Prohaska, and V. Lauwers-Cances. *"A novel three-dimensional computer-assistedmethod for a quantitative study of microvascular networks of the human cerebral cortex"*. Microcirculation,13:1-18, January 2006.

4. R. M. Cesar, Jr., E. Bengoetxea, I. Bloch, and P. Larrañaga. *"Inexact graph matching for modelbasedrecognition: Evaluation and comparison of optimization algorithms"*. Pattern Recognition, 38(11):2099-2113,2005.

5. M. A. Chaplain, S. R. McDougall, and A. R. Anderson. *"Mathematical modeling of tumor-induced angiogenesis".*Annual Review of Biomedical Engineering, 8:233-257, 2006.

6. D. Conte, P. Foggia, C. Sansone, and M. Vento. *"Thirty years of graph matching in patternrecognition"*. International Journal of Pattern Recognition and Artificial Intelligence, 18(3):265-298.

7. A. F. Frangi, R. F. Frangi, W. J. Niessen, K. L. Vincken, and M. A. Viergever. *"Multiscale vesselenhancement filtering"*. Medical Image Computing and Computer-Assisted Interventation, 1998.

8. A. A. Hagberg, D. A. Schult, and P. J. Swart. *"Exploring network structure, dynamics, and function usingNetworkX"*. In Proceedings of the 7th Python in Science Conference, Pasadena, CA, USA, August 2008.

9. H. Homann. *"Implementation of a 3D thinning algorithm"*. Insight Journal, 2007. http://hdl.handle.net/1926/1292.

10. H. Honda. *"Description of the form of trees by the parameters of the tree-like body: Effects of the branching angleand the branch length on the shape of the tree-like body"*. Journal of Theoretical Biology, 31(2):331-338, 1971.

11. J. D. Hunter. *"Matplotlib: A 2d graphics environment"*. Computing in Science and Engineering, 9(3):90-95, 2007.

12. L. Ibanez, W. Schroeder, L. Ng, and J. Cates. *"The ITK Software Guide"*. Kitware, Inc., 2005.

13. C. Kirbas and F. Quek. *"A review of vessel extraction techniques and algorithms"*. ACM Computing Surveys,36(2):81-121, 2004.

14. G. Kokai, Z. Toth, and R. Vanyi. *"Modelling blood vessels of the eye with parametric L-systems usingevolutionary algorithms"*. In Proceedings of the Joint European Conference

onArtificial Intelligence in Medicine and Medical Decision Making, Aalborg, Denmark, June 1999.

15. K. Krissian, G. Malandain, N. Ayache, R. Vaillant, and Y. Trousset. *"Model-based detection oftubular structures in 3d images"*. Computer Vision and Image Understanding, 80(2):130-171, 2000.

16. A. N. Langville and C. D. Meyer. *"Google's PageRank and Beyond: The Science of Search Engine Rankings"*.Princeton University Press, Princeton, NJ, USA, 2006.

17. A. Lindenmayer. "*Mathematical models for cellular interactions in development i. filaments with one-sided inputs"*.Journal of Theoretical Biology, 18(3):280-299, 1968.

18. A. Lindenmayer. *"Mathematical models for cellular interactions in development ii. simple and branching filamentswith two-sided inputs"*. Journal of Theoretical Biology, 18(3):300-315, 1968.

19. S. Luo and Y. Zhong. *"Extraction of brain vessels from magnetic resonance angiographic images: concise literaturereview, challenges, and proposals"*. In Proceedings of IEEE Engineering in Medicine and Biology Society, 2:1422-1425, 2005.

20. F. Nekka, S. Kyriacos, C. Kerrigan, and L. Cartilier. *"A model of growing vascular structures"*. Bulletin of Mathematical Biology, 58:409-424, May 1996.

21. W. Palubicki, K. Horel, S. Longay, A. Runions, B. Lane, R. Měch, and P. Prusinkiewicz. *"Self-organizing tree models for image synthesis"*. In Proceedings of ACM SIGGRAPH 2009, New York, NY, USA, 2009.

22. P. Ramachandran. *"MayaVi: A free tool for CFD data visualization"*. 4th Annual CFD Symposium, AeronauticalSociety of India, 2001.

23. X. Qian, M. P. Brennan, D. P. Dione, W. L. Dobrucki, M. P. Jackowski, C. K. Breuer, A. J. Sinusas, and X. Papademetris.*"A non-parametric vessel detection method for complex vascular structures"*. Medical Image Analysis, 13(1):49–61, February 2009.

24. G. Rozenberg and A. Salomaa, editors. *"Lindenmayer Systems: Impacts on Theoretical Computer Science,Computer Graphics, and Developmental Biology"*. Springer-Verlag New York, Inc., Secaucus, NJ, USA, 2001.

25. Y. Sato, S. Nakajima, N. Shiraga, H. Atsumi, S. Yoshida, T. Koller, G. Gerig, and R. Kikinis. *"Three-dimensionalmulti-scale line filter for segmentation and visualization of curvilinear structures in medical images"*. Medical Image Analysis, 2(2):143-168, 1998.

26. M. Schaap, C. T. Metz, T. van Walsum, A. G. van der Giessen, A. C. Weustink, N. R. Mollet, C. Bauer, H. Bogunovi,C. Castro, X. Deng, E. Dikici, T. O'Donnell, M. Frenay, O. Friman, M. Hernandez Hoyos, P. H. Kitslaar, K. Krissian,C. Kuhnel, M. A. Luengo-Oroz, M. Orkisz, O. Smedby, M. Styner, A. Szymczak, H. Tek, C. Wang, S. K. Warfield,S. Zambal, Y. Zhang, G. P. Krestin, and W. J. Niessen. *"Standardized evaluation methodology and reference databasefor evaluating coronary artery centerline extraction algorithms"*. Medical Image Analysis, 13(5):701-714, October 2009.

27. J. A. Sethian. *"Level Set Methods and Fast Marching Methods"*. Cambridge University Press, 1999.

28. R. Singh, J. Xu, and B. Berger. *"Global alignment of multiple protein interaction networks with application to functionalorthology detection"*. In Proceedings of the National Academy of Sciences of the United States of America. 105(35):12763-12768, September 2008.

29. M. Sofka and C. V. Stewart. *"Retinal vessel centerline extraction using multiscale matched filters, confidence andedge measures"*. IEEE Transactions on Medical Imaging, 25(12):1531–1546, Dec 2006.

30. S. Thoreson. *"An efficient solution to inexact graph matching with application to computer vision"*. PhD thesis,Norwegian University of Science and Technology, 2007.

31. N.J. Tustison, M.Siqueira, and J.C.Gee.*"N-D Linear Time Exact Signed Euclidean Distance Transform"*. InsightJournal, 2006. http://hdl.handle.net/1926/171.

32. J. R. Ullmann. *"An algorithm for subgraph isomorphism"*. Journal of ACM, 23(1):31-42, January 1976.

33. S. Worz and K. Rohr. *"Segmentation and quantification of human vessels using a 3-D cylindrical intensity model"*.IEEE Transactionson Image Processing, 16(8):1994-2004, Aug 2007.

34. P. J. Yim, P. L. Choyke, and R. M. Summers. *"Gray-scale skeletonization of small vessels in magnetic resonanceangiography"*. IEEE Transactions on Medical Imaging, 19(6):568–576, June 2000.